Water Supply

Water Supply Vol 23 No 3, 1267 doi: 10.2166/ws.2023.026

Modeling of scour depth and length of a diversion channel flow system with soft computing techniques

Nashwan K. Alomari[a], Parveen Sihag[b,*], Ahmed Mohammed Sami Al-Janabi[c] and Badronnisa Yusuf[d]

[a] Department of Dams and Water Resources Engineering, College of Engineering, University of Mosul, Mosul, Iraq
[b] Department of Civil Engineering, Chandigarh University, Mohali, Punjab, India
[c] Department of Civil Engineering, Cihan University-Erbil, Kurdistan Region, Iraq
[d] Department of Civil Engineering, Faculty of Engineering, Universiti Putra Malaysia, 43400 UPM Serdang, Selangor, Malaysia
*Corresponding author. E-mail: parveen12sihag@gmail.com

PS, 0000-0002-7761-0603

ABSTRACT

This study employed soft computing techniques, namely, support vector machine (SVM) and Gaussian process regression (GPR) techniques, to predict the properties of a scour hole [depth (ds) and length (Ls)] in a diversion channel flow system. The study considered different geometries of diversion channels (angles and bed widths) and different hydraulic conditions. Four kernel function models for each technique (polynomial kernel function, normalized polynomial kernel function, radial basis kernel, and the Pearson VII function kernel) were evaluated in this investigation. Root mean square error (RMSE) values are 8.3949 for training datasets and 11.6922 for testing datasets, confirming that the normalized polynomial kernel function-based GP outperformed other models in predicting Ls. Regarding predicting ds, the polynomial kernel function-based SVM outperforms other models, recording RMSE of 0.5175 for training datasets and 0.6019 for testing datasets. The sensitivity investigation of input parameters shows that the diversion angle had a major influence in predicting Ls and ds.

Key words: diversion angle, diversion channel, scour depth, scour length, soft computing

HIGHLIGHTS

- Soft computing implementation for prediction of the properties of scour hole.
- Benchmarking of SVM and GP-based data-intelligent models.
- The diversion angle had a major influence in predicting the properties of scour hole.

1. INTRODUCTION

The use of unlined diversion channels for irrigation, domestic, or hydropower projects has introduced concern over the scouring of the beds of such channels. The scouring reduces the cover of related hydraulic structures' foundations due to sediment transport; thereby influencing their stability (Hoffmans & Pilarczyk 1995; Khwairakpam & Mazumdar 2009). Diversion channels may occur naturally as well in rivers, known as river bifurcations; however, they are commonly unstable, evolve in time splits, and merge due to the annual dynamics of river geomorphology (Kleinhans *et al.* 2013; Herrero *et al.* 2015; Redolfi *et al.* 2016).

Owing to the importance of flow behavior in diversion channels for water and sedimentation management, numerous studies (Ramamurthy & Satish 1988; Ramamurthy *et al.* 1990; Hsu *et al.* 2002; Mignot *et al.* 2013, 2014; Seyedian *et al.* 2014; Xu *et al.* 2016; Momplot *et al.* 2017) have been conducted to investigate different phenomena that accompany diversion flow. Despite the presence of bed morphology as a very important factor in designing diversion channels (Xu *et al.* 2016), the majority of these researches are about diversion channels with rigid boundary conditions, while the effects of bed morphology in unlined diversion channels were ignored.

Flow in diversion channels with sand bed conditions was studied by Barkdoll *et al.* (1999), Dehghani *et al.* (2009), Herrero *et al.* (2015), Alomari *et al.* (2018), Abdalhafedh & Alomari (2021), and different diversion angles were considered by Keshavarzi & Habibi (2005) and Alomari *et al.* (2020). Although Barkdoll *et al.* (1999) and Herrero *et al.* (2015) investigated

flow in unlined diversion channels with a diversion angle of 90°, Alomari *et al.* (2020) found that the diversion channel received maximum water discharge and minimum sediment discharge when its diversion angle was 30° or 45° among 90°, 75°, 60°, 45°, and 30° diversion angles. Moreover, the optimum diversion angle based on intake separation zone size was found to be at an angle of 55°, as reported by Keshavarzi & Habibi (2005).

Several studies (Nakato 1984; Kerssens & van Urk 1986; Nakato *et al.* 1990; Nakato & Ogden 1998; Michell *et al.* 2006) were conducted to investigate the effect of sediment transport in diversion channels, and hence, several physical hydraulic models were provided. Furthermore, the minimum foundation depth that is safe from the effects of scour in rivers and unlined bed channels has been studied for many hydraulic structure types, such as rock structures (Pagliara *et al.* 2016), pile groups (Amini *et al.* 2012), complex piers (Amini *et al.* 2011; Solaimani *et al.* 2017), submerged obstacles (Euler & Herget 2012), and spur dykes (Duan *et al.* 2009). Moreover, a scour hole was observed by Barkdoll *et al.* (1999), Herrero *et al.* (2015), Alomari *et al.* (2018, 2020) at the bed of the main channel down diversion channel conjunction due to the secondary vortex.

Since the presence of soft computing techniques to deal with different time-consuming and difficult engineering problems, (Taylor & Meldrum 1994; Duch 2007; Aggarwal *et al.* 2013; Liu *et al.* 2017; Dibs *et al.* 2018), different soft computing models, such as support vector machines (SVM), random forest (RF), and Gaussian process regression (GPR) have been employed to solve various water resources engineering problems (Ehteram *et al.* 2021; Sihag *et al.* 2021; Yaseen *et al.* 2021) and they are recommended to be applied for analyzing scour depth and length problems (Moradi *et al.* 2019).

The main objective of this study is to evaluate the performance of two soft computing techniques, namely, SVM and GPR, in predicting the properties of scour holes [scour depth (ds) and scour length (Ls)] due to diversion channels with considering different geometries of diversion channels (angles and bed widths). Moreover, the effects of water flow, depth, and velocity in the main channel on (ds) and (Ls) were considered in this study.

2. METHODOLOGY

2.1. Experimental set-up

Data used for modeling scour holes due to the diversion flow system were based on experimental work that was conducted using a rectangular diversion channel with a 2.75-m length, 0.6-m depth, and adjustable bed widths of 0.15, 0.12, and 0.09 m. This channel was diverted from the left side wall of the main channel, about at the middle of the working section, which is filled with sand. The dimensions of the main channel are 12.5-m length, 0.313-m width, and 0.6-m depth (Figure 1). The diversion channel was built to be flexible and angle adjustable with the main channel.

The sand was used for the bed of the diversion and main channels with a medium particle diameter of 0.4 mm ($\sigma_g = 1.46$ and $\rho_s = 2{,}530$). The sand layer was 0.18 m thick and prior to starting each experiment, the bed was checked, filled, and flattened. Flow in the diversion channel system was re-circulated by collecting water and sediment at the system's ends and pushing it back into the system. A flow meter was fitted at the pumping pipe to measure the overall discharge and a control valve was used to regulate the overall discharge.

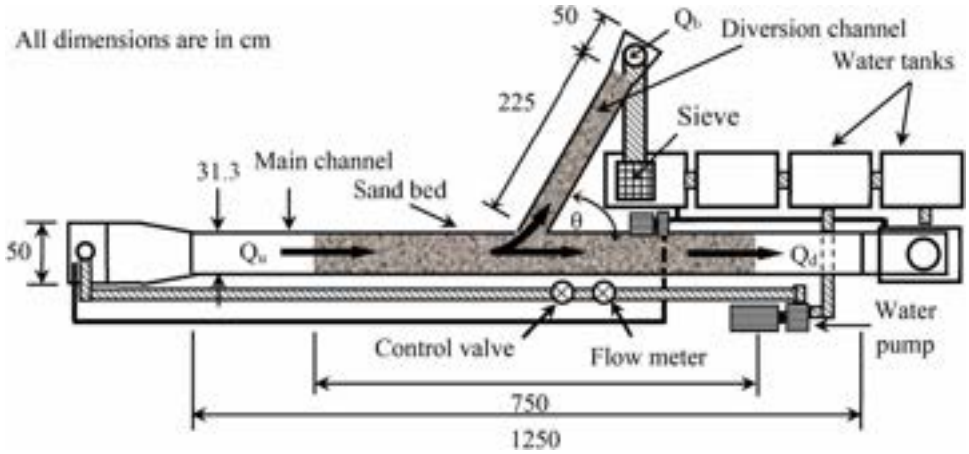

Figure 1 | Main and diversion channel layout.

To alleviate flow turbulence, a mesh was added at the main channel entry. Moreover, the surface of the soil at the inlet and outlets of the working section was covered by paces of Perspex to protect against the local scour. Controlling the discharge of the diversion channel flow was accomplished by inserting teeth-shaped pieces with 30% flow opening and 70% contraction at the ends of both channels. Using the teeth-shaped components helps to control the ratio of diversion to total discharge and lets the sand move through the channels without getting stuck at the channel's outlets. At selected points, the depth of the water and the scour were measured with precision up to parts of a millimeter using a vertical point gauge. Scour depth was measured in 30-min time intervals at the first 2 h, then once each hour.

2.2. Experimental tests

A total of 75 experiments were accomplished experimentally as detailed in Table 1. Throughout each experiment, the discharge in the diversion channel was measured using the volumetric approach and the discharge in the downstream main channel (Qd) was determined using the continuity equation. Before each experiment, the sand bed was smoothed. Then, an experiment was started by closing the channel's outlets and gently supplying the water to an appropriate depth into the channels and then opening the outlets by setting the desired discharge. Each experiment lasted 12 h to complete. The temperature in the laboratory was kept at around (27 °C $\pm$ 1.5 °C) throughout the study.

2.3. Soft computing analysis

The effectiveness of two soft computing techniques, namely, SVM and GPR, in predicting the length and depth of the scour in the diversion channel flow system was evaluated. The details of the two soft computing techniques are presented below.

2.3.1. Support vector machines

As per Cortes & Vapnik (1995), the SVM can be described as classification and regression methods, which are derivatives of the theory of statistical learning. The concept of optimum class separation serves as a major base for the SVM classification methods. If the classes are separable, it has been suggested that this technique chooses, among an unlimited quantity of linear classifiers, the one that records the minimum error, resulting from structural risk minimization. Hence, the carefully chosen hyperplane would leave the greatest error between the two classes (Cortes & Vapnik 1995).

If both classes are inseparable, SVM will attempt to locate the hyperplane that simultaneously maximizes the margin and minimizes a quantity proportional to the number of misclassification errors. A positive constant must be chosen beforehand; it determines the tradeoff between margin error and misclassification error. There can be a further extension of this particular technique of designing an SVM for the countenance of the nonlinear decision surfaces. Cortes & Vapnik (1995) have suggested that this can be consummated by the projection of the variables (original set) into a higher dimensional feature space and by the formulation of a linear grouping problem in the feature space.

Cortes & Vapnik (1995) suggested the ε support vector regression (SVR) through the introduction of an alternative ε insensitive loss function. The resolution of the SVR, as suggested by Smola (1996), is to develop a function that has the smallest possible divergence from the actual target vectors for all training data and that is as flat as feasible. The conception of the nonlinear support vector kernel function for regression is additionally presented by Cortes & Vapnik (1995). Readers can refer to Cortes & Vapnik (1995) and Smola (1996) for more details about the SVR. Fewer user-defined parameters are the prerequisites for SVR. SVR needs the configuration of kernel-specific factors, as well as, the selection of a kernel. In addition, it is necessary to calculate the appropriate regularization parameter C and error size in the sensitive zone ε. The selection of parameters governs the intricacy of extrapolation.

Table 1 | Details of experimental tests

Diversion angle (θ°)	Bb/Bm = Br (%)[a]	Total discharge, Qu (L/s)
30		
45		
60	29, 38, and 48	7.25, 8.5, 9.75, 11, and 12.25
75		
90		

[a]Bb/Bm is the bed width ratio of the main channel to the diversion channel.

2.3.2. Gaussian process regression

According to Neal (2000), Gaussian processes (GP) may be termed as a generality of the Gaussian distribution and here vector is the mean and the matrix serves as the covariance. GP regression is an expedient approach to nonparametric regression owing to its theoretical simplicity as well as its worthy generalization capability and it provides an output that is probabilistic (Williams & Rasmussen 2006).

In GP regression, for each $\boldsymbol{X}_*$, which is defined as the vector of the test data, the predicted distribution of the output is $\boldsymbol{Y}_*/(\boldsymbol{X},\ \boldsymbol{Y}),\ \ \boldsymbol{X}_* \sim N(\mu,\ \Sigma)$ and it is presented as:

$$\mu = K\ (\boldsymbol{X}_*, \boldsymbol{X})\ (K\ (\boldsymbol{X}, \boldsymbol{X}) + \sigma^2 \boldsymbol{I})^{-1} \boldsymbol{Y} \tag{1}$$

$$\Sigma = K\ (\boldsymbol{X}_*, \boldsymbol{X}_*) - \sigma^2 I - K\ (\boldsymbol{X}_*,\ \boldsymbol{X})\ (K\ (\boldsymbol{X}, \boldsymbol{X}) + \sigma^2 I)^{-1} K\ (\boldsymbol{X}, \boldsymbol{X}_*) \tag{2}$$

where σ^2 is the degree of noise, $\boldsymbol{I}$ is the identity matrix, and y would be established as $y \sim f(x) + \xi$, where $\xi \sim N\ (0,\ \ \sigma^2)$, the character $\sim$ stands for sampling.

For every input x in GP regression, an accidental variable $f(x)$ represents the amount of the stochastic function f at that point is attached. Another assumption, which is the error ξ in the observations, it is typically self-determining and identically distributed, with a mean of zero $(\mu(x) = 0)$, a variance of σ^2 and $f(x)$ drawn from the Gaussian process is determined χ by the parameter k.

$$Y = (y_1,\ \ \ldots\ldots\ldots y_n) \sim N\ (0,\ K + \sigma^2 \boldsymbol{I}) \tag{3}$$

where $K_{ij} = K\ (x_i,\ x_j)$ and $\boldsymbol{I}$ is the identity matrix.

The data were divided into two sets, training and testing dataset, as n and n_*, respectively. Then, the covariance matrix-$(n \times n_*)$ to evaluate all two sets, which is characterized as $K\ (\boldsymbol{X}, \boldsymbol{X}_*)$ and in a comparable fashion, this applies to the other amounts of $K\ (\boldsymbol{X}, \boldsymbol{X})$, $K\ (\boldsymbol{X}_*,\ \boldsymbol{X})$, and $K\ (\boldsymbol{X}_*, \boldsymbol{X}_*)$; here $\boldsymbol{X}$ and $\boldsymbol{Y}$ are the vectors of both of the training data and labels y_i (Yetilmezsoy *et al.* 2021).

For the generation of a positive quasi covariance matrix K, here $K_{ij} = K\ (x_i, x_j)$, a quantified covariance function is necessary. The terms kernel function and covariance function, which are both utilized in SVM and GP regression, are interchangeable. By identifying both degrees of noise (σ^2) and kernel function, it would be enough to have Equations (1) and (2) for inference purposes. Throughout the GP regression model training process, the user has to pick out an opposite covariance function, the parameters of it as well as the degree of noise. In the situation of GP regression with Gaussian noise having a constant value, a GP model may be constructed using Bayesian inference. After minimizing the negative log-posterior, the equation will be:

$$p\ (\sigma^2,\ k) = \frac{1}{2} Y^T\ (K + \sigma^2 I)^{-1} Y + \frac{1}{2} \log|K + \sigma^2 I| - \log p\ (\sigma^2) - \log\ p\ (k) \tag{4}$$

For determining the hyperparameters, Equation (4) follows a partial derivative regarding σ^2 , k, and minimization can be with the assistance of gradient descent. Kuss (2006) has published a comprehensive descriptive account of the GP regression in addition to different covariance functions.

2.3.3. Details of kernel function

The kernel function idea is used in the creation of the SVM and GP-based regression approaches (Mehdipour *et al.* 2018; Sihag *et al.* 2018, 2019). The four most frequently used kernel functions: a polynomial kernel function ($K\ (x,\ x') = ((x\ .\ x') + 1)^{d*}$), normalized polynomial kernel function $\left(K_{\text{cosine}}(x, x') = K\ (x, x')/\sqrt{K(x, x).K(x', x')}\right)$, radial basis kernel ($K\ (x\ ,\ x') = e^{-\gamma|x-x'|^2}$), and the Pearson VII function kernel $\left(1/\left[1 + \left(2\sqrt{\|x_i - x_j\|^2}\sqrt{2^{(1/\omega)} - 1}/\sigma\right)^2\right]^{\omega}\right)$, where d^*, γ, σ, and ω are kernel-specific parameters.

2.4. Dataset

To develop the soft computing models, data preparation is the first step. The collected dataset is split into training and testing groups, which were randomly assigned. The training dataset is utilized for model development, whereas the testing dataset is utilized for model validation. Table 2 provides the range of datasets assigned for training and testing. A total of 75 datasets were collected, 53 datasets for training, and 22 datasets are utilized for testing the developed models. Total discharge (Qu), diversion channel bed width (Bb), the critical velocity of the beginning of motion of bed materials (Vc), the ratio of the main channel bed width to the diversion channel bed width (Br = Bb/Bm), diversion to main channel water discharge (Qr), water depth in the main channel at upstream (yu), main channel velocity of the flow at upstream (Vu), and sine of diversion channel angle (Sin θ) were considered as input parameters whereas scour length (Ls) and scour depth (ds) at was considered as a target.

2.5. Model performance indices parameters

The performance of models was evaluated using five widely used statistical performance indicators, namely, the correlation coefficient (CC), root mean square error (RMSE), mean absolute error (MAE), Nash Sutcliffe model efficiency (NS), and scattering index (SI) as presented by Equations (5)–(9). The performance evaluation includes both training and testing datasets.

$$\mathrm{CC} = \frac{\sum_{i=1}^{N}(P_i - \bar{P})(O_i - \bar{O})}{\sqrt{\sum_{i=1}^{N}(P_i - \bar{P})^2 \sum_{i=1}^{N}(O_i - \bar{O})^2}} \tag{5}$$

$$\mathrm{MAE} = \frac{1}{N}\sum_{i=1}^{N}|P_i - O_i| \tag{6}$$

$$\mathrm{RMSE} = \sqrt{\frac{1}{N}\sum_{i=1}^{N}(P_i - O_i)^2} \tag{7}$$

$$\mathrm{NS} = 1 - \left(\frac{\sum_{i=1}^{N}(P_i - O_i)^2}{\sum_{i=1}^{N}(O_i - \bar{O})^2}\right) \tag{8}$$

$$\mathrm{SI} = \frac{\mathrm{RMSE}}{\bar{O}} \tag{9}$$

Table 2 | Range of assigned dataset

	Training dataset					Testing dataset				
Parameters	**Min.**	**Max.**	**Mean**	**StD**	**CL (95%)**	**Min.**	**Max.**	**Mean**	**StD**	**CL (95%)**
Qu (L/s)	7.250	12.250	9.7736	1.7246	0.4754	7.250	12.250	9.693	1.947	0.8633
Bb (cm)	9.000	15.000	12.000	2.4962	0.6880	9.000	15.000	12.000	2.4495	1.086
Vc (m/s)	0.212	0.233	0.2236	0.0055	0.0015	0.213	0.233	0.2233	0.0064	0.0028
Br (%)	28.571	47.619	38.095	7.9243	2.1842	28.571	47.619	38.095	7.776	3.4478
Qr (%)	18.480	31.180	24.959	4.0168	1.1072	18.210	31.180	24.820	4.2436	1.8815
yu (cm)	8.200	12.850	10.535	1.2631	0.3481	8.350	12.900	10.493	1.4828	0.6574
Vu (m/s)	0.224	0.584	0.3716	0.0997	0.0275	0.223	0.5739	0.3752	0.1036	0.0459
Sin θ	0.500	1.000	0.8054	0.1867	0.0515	0.500	1.000	0.8135	0.1876	0.0832
Ls (cm)	33.25	118.05	68.759	21.5925	5.9516	31.650	113.30	71.079	23.214	10.2925
ds (cm)	7.10	17.50	12.005	2.3036	0.6350	6.500	15.900	12.084	2.2146	0.9819

where O_i and P_i are, respectively, the observed and the predicted parameter, $\bar{O}$ is the average observed parameter and n is the number of the observed data.

Furthermore, two graphical performance assessment methods, the Taylor diagram and the box plot are also plotted for the comparison of applied models. Taylor diagrams depict the similarity between two patterns and the degree to which a model pattern corresponds to the actual pattern (Taylor 2001). Box plots have been also selected for assessment. It uses five descriptive statistics, such as lower, median, and upper quartile, beside the minimum and maximum in a graphical presentation.

3. RESULTS AND DISCUSSION

3.1. Assessment of SVM-based model for the prediction of Ls

Table 3 presents the performance indices parameters, which are used to measure the prediction accuracy of the different prediction models. From Table 3, for all SVM-based models, the performance evaluation parameters values in predicting Ls using training and testing stages suggest that the polynomial kernel function-based SVM model outperforms other kernels, function-based SVM models, in predicting Ls with RMSE values as 8.5265 and 12.0189, MAE values as 6.3916 and 9.1556, CC values as 0.9173 and 0.8672, NS values as 0.8411 and 0.7192, and SI values as 0.1240 and 0.1691 for both datasets (training and testing), respectively. Figure 2 presents the plot of the agreement and error. Furthermore, it presents the models performance. These plots suggest that the polynomial kernel function-based SVM model predicted values are nearby the perfect agreement line and follow the same pathway as actual values with the least amount of divergence compared with other kernel function-based SVM models.

Various kernel function-based SVM models were compared using the Taylor diagram as shown in Figure 3, which is based on RMSE, CC, and standard deviation, where the outperforming model is the one nearby to the actual point. The outcomes of Taylor diagrams show that the SVM_Poly model is the highest in accuracy compared with other models, which were applied to predict Ls. To evaluate the inconsistency of most Ls predictions besides the actual values, the 25, 50, and 75% quartile values of the actual and predicted Ls are assessed using Table 4. Table 4 indicates that the SVM_Poly model has closer quartiles to the actual values compared with other kernel function-based SVM models. The interquartile range (IQR) of SVM_Poly is also nearer to the IQR of actual data.

Table 3 | Performance indices parameters for SVM and GP-based models for the prediction of Ls

Approaches	CC	RMSE	MAE	NS	SI
	Training dataset				
SVM_Poly	0.9173	8.5265	6.3916	0.8411	0.1240
SVM_NPoly	0.8950	9.7084	6.6587	0.7940	0.1412
SVM_PUK	1.0000	0.0907	0.0800	1.0000	0.0013
SVM_RBF	0.9516	6.5801	3.7695	0.9053	0.0957
GP_Poly	0.9167	11.9806	6.8399	0.8402	0.1742
GP_NPoly	0.9201	8.3949	5.9964	0.8459	0.1221
GP_PUK	1.0000	0.2385	0.1941	0.9999	0.0035
GP_RBF	0.9782	4.4620	3.3245	0.9565	0.0649
	Testing dataset				
SVM_Poly	0.8672	12.0189	9.1556	0.7192	0.1691
SVM_NPoly	0.8090	13.6417	10.4960	0.6382	0.1919
SVM_PUK	0.8643	12.9722	11.1883	0.6729	0.1825
SVM_RBF	0.8601	12.7411	9.5466	0.6844	0.1793
GP_Poly	0.8614	16.5979	9.6998	0.7200	0.2335
GP_NPoly	0.8744	11.6922	9.0375	0.7342	0.1645
GP_PUK	0.8643	12.9855	11.2002	0.6722	0.1827
GP_RBF	0.8621	13.3579	10.9985	0.6531	0.1879

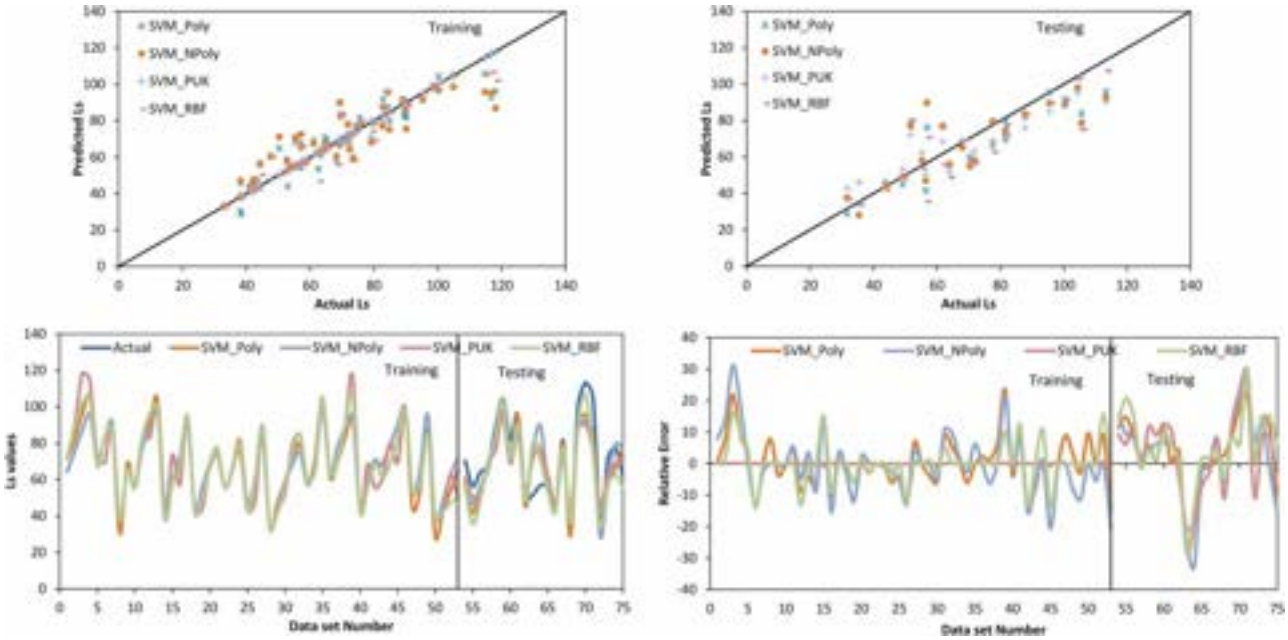

Figure 2 | SVM-based model performance for predicting the Ls.

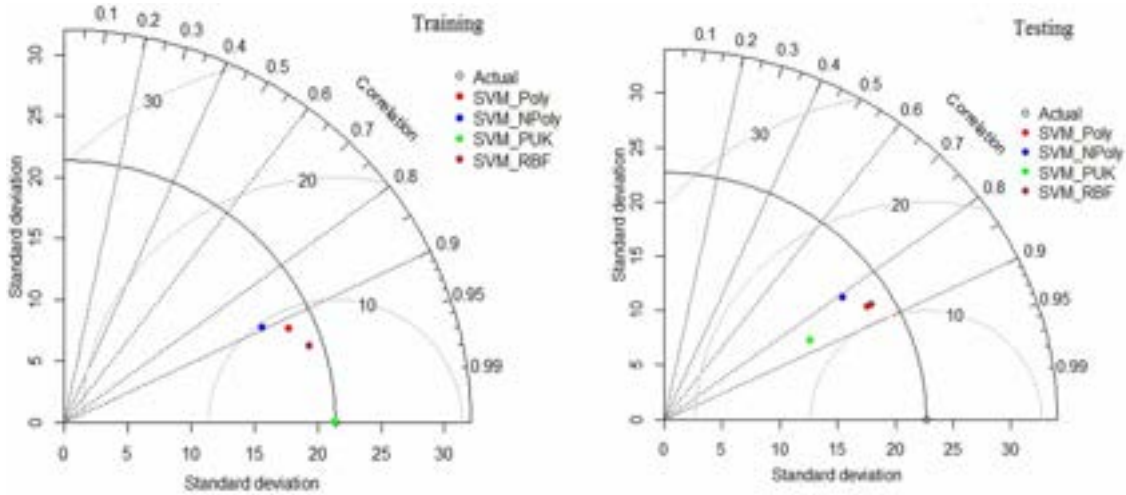

Figure 3 | Taylor diagram for various kernel function-based SVM models used for prediction of Ls using both datasets (training and testing).

3.2. Assessment of GP-based model for the prediction of Ls

Table 3 presents five performance indices parameters that were performed for the evaluation of the predictive accuracy of all GP-based models for Ls prediction. Four kernel functions were used for the GP-based models' development. Results of Table 3 suggest that the normalized polynomial kernel function-based GP model outperforms other kernel function-based GP models for Ls prediction with RMSE values of 8.3949 and 11.6922, MAE values as 5.9964 and 9.0375, CC values as 0.9201 and 0.8744, NS values as 0.8459 and 0.7342, and SI values as 0.1221 for training stage and 0.1645 for testing stage. Figure 4 presents the plot of the agreement and error. Furthermore, it presents the models performance. These plots suggest that the normalized polynomial kernel function-based GP model predicted values are nearby the perfect agreement line. Moreover, it follows the same pathway as actual values with the least amount of divergence compared with other kernel function-based GP models.

Table 4 | Descriptive statistics of actual and predicted values using GP and SVM-based models for the prediction of Ls

Statistic	Minimum	Maximum	First Quartile	Mean	Third Quartile	IQR
	Training dataset					
Actual	33.2500	118.0500	53.0000	68.7594	82.9000	29.9000
SVM_Poly	28.7480	105.7670	55.3790	68.7991	82.8650	27.4860
SVM_NPoly	33.0850	98.6050	56.9040	69.1282	82.4800	25.5760
SVM_PUK	33.3770	117.9000	53.0740	68.7586	82.9820	29.9080
SVM_RBF	33.4130	106.6770	55.2540	68.5379	84.4980	29.2440
GP_Poly	32.5540	109.8290	53.4510	68.9407	83.8120	30.3610
GP_NPoly	29.3760	103.1920	55.1060	68.7377	86.5710	31.4650
GP_PUK	33.5230	117.3450	53.0840	68.7599	83.2230	30.1390
GP_RBF	33.2520	114.4150	55.4980	68.7554	81.8270	26.3290
	Testing dataset					
Actual	31.6500	113.3000	55.5500	71.0795	86.2250	30.6750
SVM_Poly	28.9200	103.5730	55.6640	67.7903	81.4423	25.7783
SVM_NPoly	28.1200	98.0590	55.2615	68.2825	82.6013	27.3398
SVM_PUK	42.7130	95.3540	55.3488	67.5545	76.0533	20.7045
SVM_RBF	33.8080	107.3110	50.0443	65.9115	79.3268	29.2825
GP_Poly	35.3810	107.5230	52.6613	67.7335	81.0240	28.3628
GP_NPoly	28.7720	102.8350	54.5743	67.2309	81.6085	27.0343
GP_PUK	42.8760	95.2580	55.4145	67.5934	76.0918	20.6773
GP_RBF	33.0290	116.3420	43.7145	64.5294	75.4365	31.7220

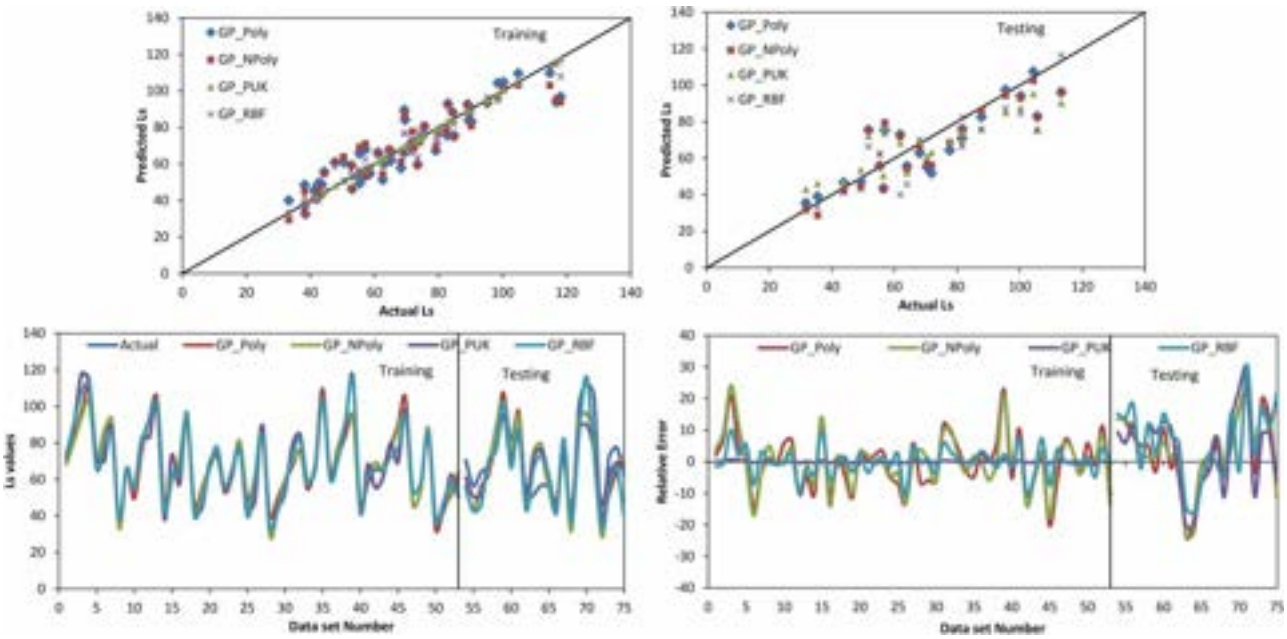

Figure 4 | GP-based model performance for predicting the Ls.

The outcomes of the illustration in Figure 5 of the Taylor diagram recommend that the GP_NPoly model (solid blue circle) outperformance other models in prediction Ls. To evaluate the inconsistency of most Ls predictions besides the actual values, the 25, 50, and 75% quartile values of the actual and predicted Ls are assessed using Table 4. Table 4 displays that the GP_NPoly model has closer quartiles to the actual values compared with other kernel function-based SVM models. The IQR of GP_NPoly is also closer to the IQR of actual data.

3.3. Assessment of SVM-based model for ds prediction

Table 5 presents the performance indices parameters, which are usually used to measure the prediction accuracy of the different models. The same four kernel functions were used for SVM-based model development for ds as selected for Ls prediction model development. Table 5 shows the performance indices parameters (CC, RMSE, MAE, NE, and SI) values for all SVM-based models for ds prediction for the training stage and testing stage. Table 5 shows that the polynomial kernel function-based SVM model outperforms other kernel function-based SVM models in ds prediction with RMSE values of 0.5175 and 0.6019, MAE values of 0.3563 and 0.4531, CC values of 0.9746 and 0.9710, NS values of 0.9486 and 0.9226, and SI values of 0.0431 and 0.0498 for the training and testing stages, respectively. Figure 6 presents the plot of the agreement and error. Furthermore, it presents the models' performance. These plots suggest that the SVM-Poly model predicted values are close to the perfect agreement line and follow the same pathway as actual values with the least amount of divergence compared with the other kernel function-based SVM models.

Various kernel function-based SVM models were compared using the Taylor diagram as shown in Figure 7. From the diagram, the SVM_Poly model (solid red circle) has the highest precision of other kernel function-based SVM models for the prediction of ds. To evaluate the inconsistency of the most ds predictions besides the actual values, the 25, 50, and 75% quantile values of the actual and predicted ds are assessed using Table 6. Table 6 indicates that the SVM_Poly model has closer quartiles to the actual values compared with other kernel function-based SVM models. The IQR of SVM_Poly is also closer to the IQR of actual data.

3.4. Assessment of GP-based model for the prediction of ds

GP-based model development for ds prediction was done using the same four kernel functions, as selected for Ls prediction model development (Table 5). From Table 5, the polynomial kernel function-based GP model records better performance than other kernel function-based GP models for ds prediction with RMSE values of 0.6772 and 0.6033, MAE values of 0.3527 and 0.5182, CC values of 0.9775 and 0.9663, NS values of 0.9551 and 0.9222, and SI values of 0.0564 and 0.0499 for training and testing stages, respectively. Figure 8 presents the plot of the agreement and error. Furthermore, it presents the models' performance. These plots suggest that the GP_Poly model predicted values are nearby of the perfect agreement

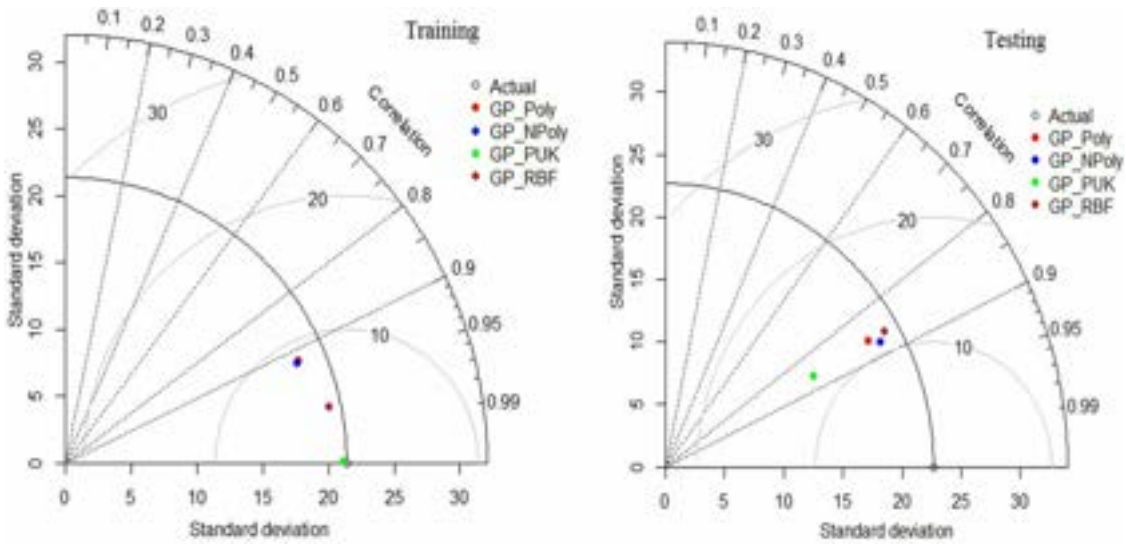

Figure 5 | Taylor diagram for various kernel function-based GP models used for prediction of Ls using both datasets (training and testing).

Table 5 | Evaluation of the parameter's performance for SVM and GP-based models for ds prediction

Approaches	CC	RMSE	MAE	NE	SI
	Training dataset				
SVM_Poly	0.9746	0.5175	0.3563	0.9486	0.0431
SVM_NPoly	0.9647	0.6284	0.4166	0.9241	0.0523
SVM_PUK	1.0000	0.0106	0.0096	1.0000	0.0009
SVM_RBF	0.9875	0.3711	0.2192	0.9736	0.0309
GP_Poly	0.9775	0.6772	0.3527	0.9551	0.0564
GP_NPoly	0.9834	0.4158	0.3193	0.9668	0.0346
GP_PUK	1.0000	0.0228	0.0171	0.9999	0.0019
GP_RBF	0.9956	0.2156	0.1652	0.9911	0.0180
	Testing dataset				
SVM_Poly	0.9710	0.6019	0.4531	0.9226	0.0498
SVM_NPoly	0.9258	0.8772	0.7410	0.8356	0.0726
SVM_PUK	0.9412	1.0725	0.7749	0.7543	0.0888
SVM_RBF	0.9610	0.6570	0.5412	0.9078	0.0544
GP_Poly	0.9663	0.6033	0.5182	0.9222	0.0499
GP_NPoly	0.9481	0.7562	0.6475	0.8779	0.0626
GP_PUK	0.9404	1.0796	0.7794	0.7510	0.0893
GP_RBF	0.9540	0.6943	0.5589	0.8970	0.0575

line. It follows the same pathway as actual values with the least amount of divergence as a compression with the other kernel function-based GP models. Taylor diagram is also plotted to compare various kernel function-based GP models (Figure 9). The results of Taylor diagrams confirm that the GP_Poly model (solid red circle) has the highest precision of other kernel function-based GP models in ds prediction.

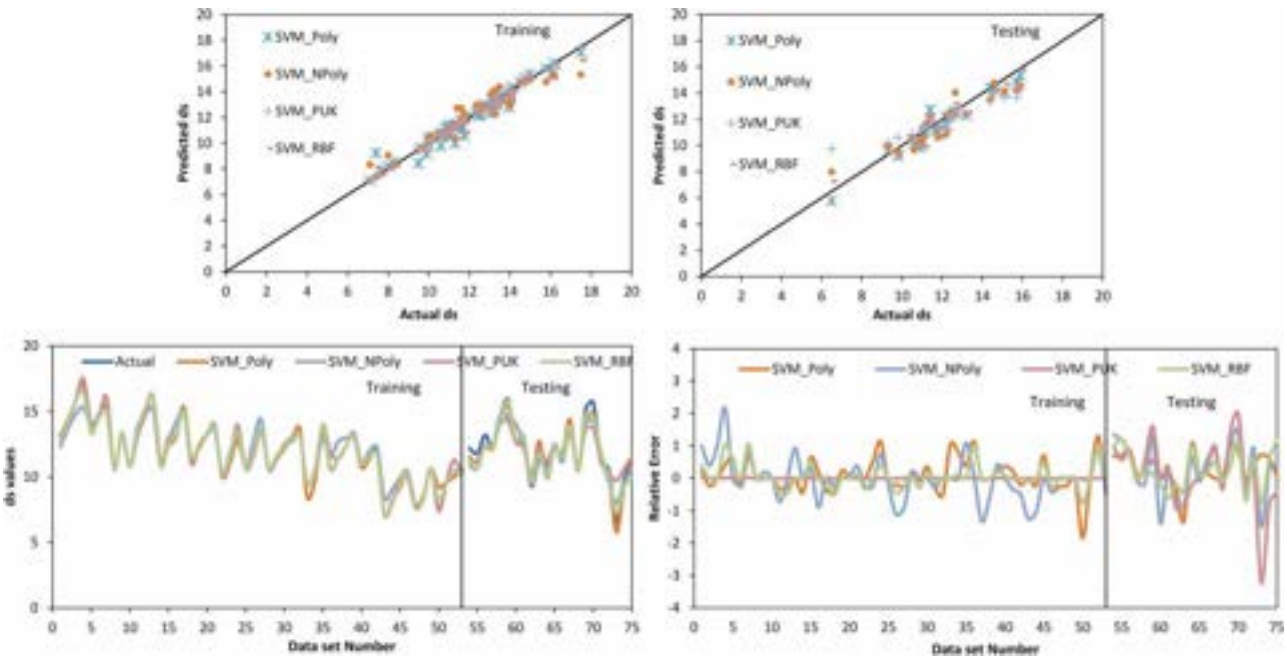

Figure 6 | SVM-based model performance for predicting the ds.

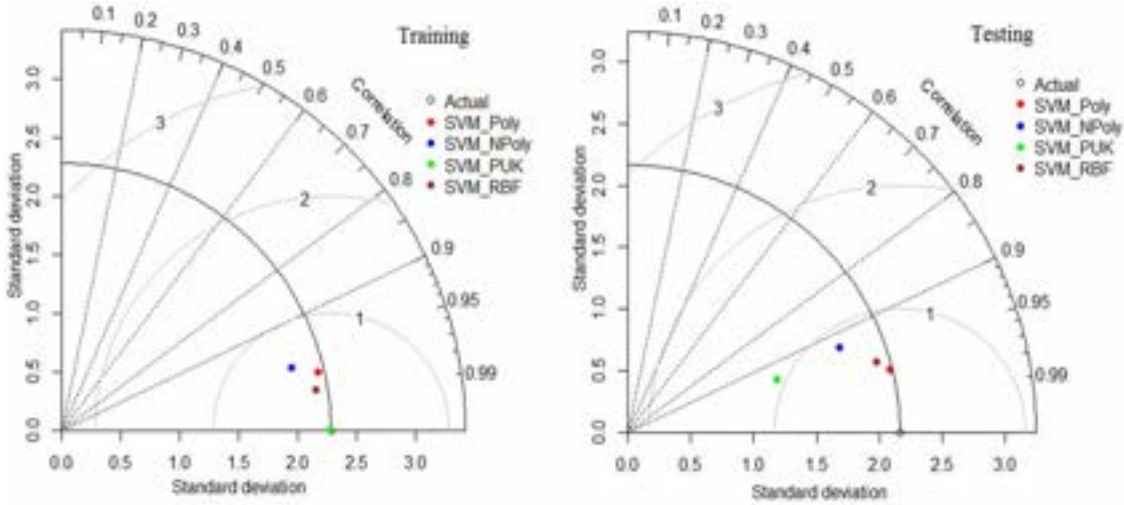

Figure 7 | Taylor diagram for various kernel function-based SVM models used for prediction of ds using both datasets (training and testing).

To evaluate the discrepancy of the most ds prediction besides the actual values, the 25, 50, and 75% quartile values of the actual and predicted ds are assessed using Table 6. Table 6 shows that the GP_Poly model has closer quartiles to the actual values compared with other kernel function-based SVM models. The (IQR of GP_Poly is also closer to the IQR of actual data.

3.5. Intercomparing of developed models

Prediction of the target values using a soft computing-based model is easy, reasonable, and more time-saving than performing experimentation. Soft computing-based models mainly depend on past data, which is used for model preparation. During this

Table 6 | Descriptive statistics of actual and predicted values using GP and SVM-based models for ds prediction

Statistic	Minimum	Maximum	First Quartile	Mean	Third Quartile	IQR
	Training dataset					
Actual	7.1000	17.5000	10.6000	12.0047	13.4000	2.8000
SVM_Poly	7.1010	17.0800	10.5800	11.9252	13.3910	2.8110
SVM_NPoly	7.4160	15.3300	10.6200	12.0099	13.2320	2.6120
SVM_PUK	7.1050	17.4900	10.6110	12.0056	13.3900	2.7790
SVM_RBF	7.2010	16.4540	10.6000	11.9480	13.4390	2.8390
GP_Poly	7.3370	17.1210	10.4600	12.0312	13.3840	2.9240
GP_NPoly	7.5080	16.3010	10.6540	12.0063	13.4500	2.7960
GP_PUK	7.1560	17.4390	10.6120	12.0050	13.3920	2.7800
GP_RBF	7.1570	17.0590	10.6180	12.0060	13.4540	2.8360
	Testing dataset					
Actual	6.5000	15.9000	10.9875	12.0841	13.0625	2.0750
SVM_Poly	5.7780	15.3610	10.6213	11.7792	12.7130	2.0918
SVM_NPoly	7.9930	14.7810	10.5963	11.8257	13.2755	2.6793
SVM_PUK	9.7290	14.2950	11.1855	11.9570	12.5828	1.3973
SVM_RBF	7.2620	15.7910	10.1173	11.8129	13.1218	3.0045
GP_Poly	5.9750	15.6080	10.5605	11.8541	12.9935	2.4330
GP_NPoly	7.1240	15.3840	10.3128	11.7725	13.3313	3.0185
GP_PUK	9.7720	14.2910	11.1998	11.9669	12.5768	1.3770
GP_RBF	7.2440	15.8720	10.2078	11.8367	13.2750	3.0673

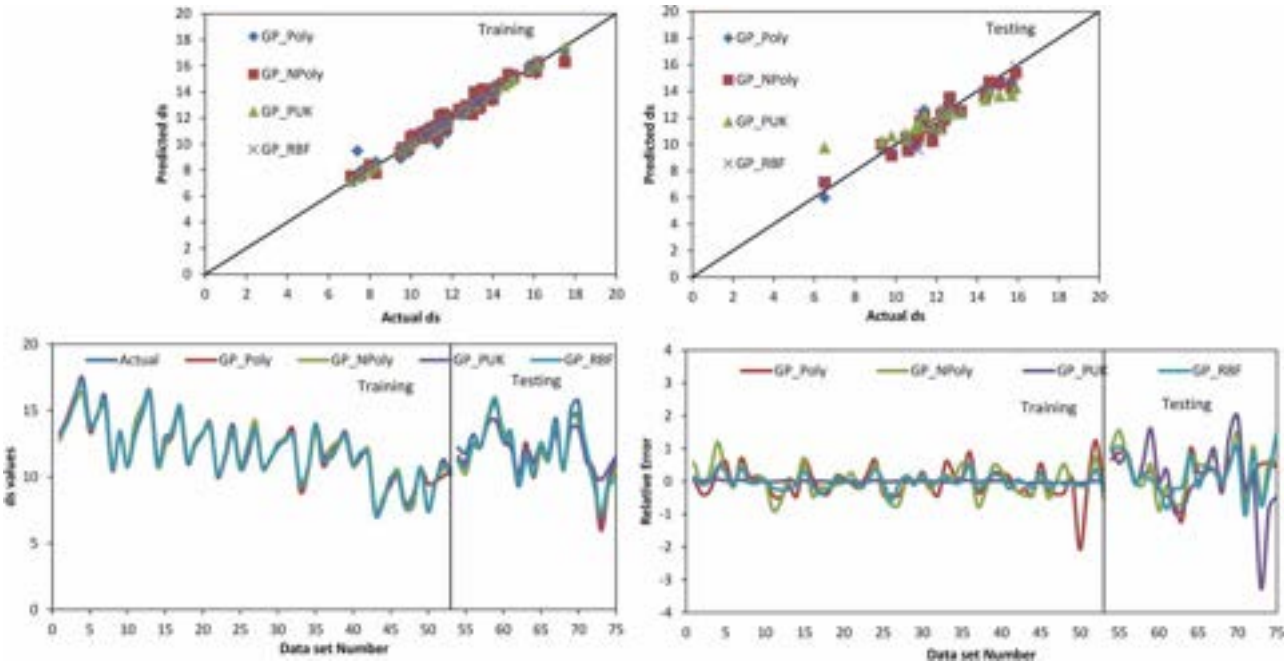

Figure 8 | SVM-based model performance for predicting the ds.

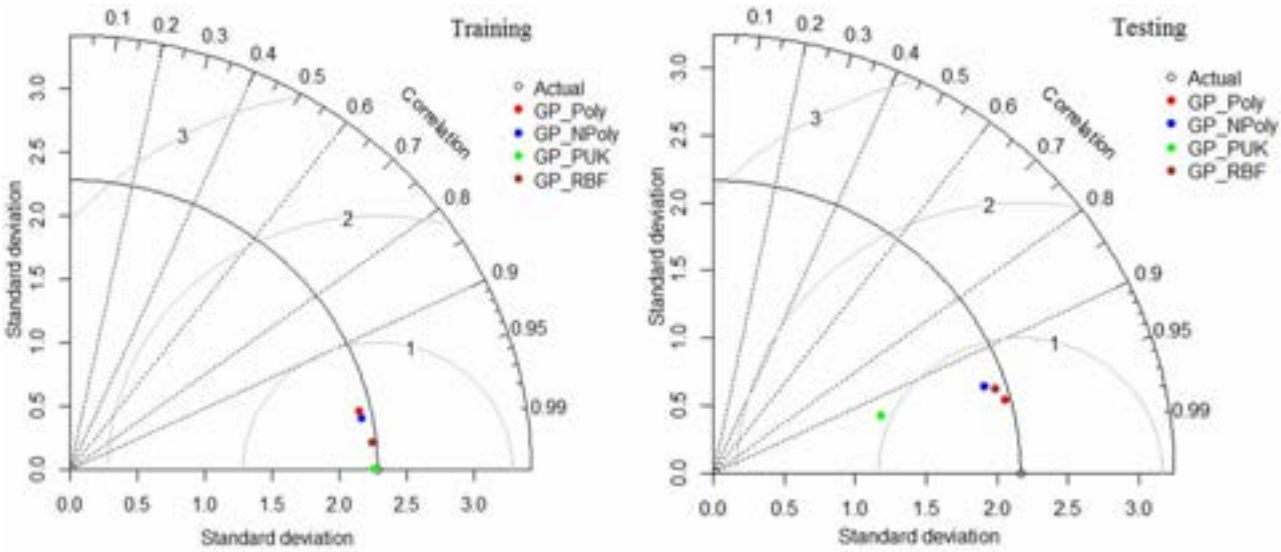

Figure 9 | Taylor diagram for various kernel function-based GP models used for prediction of ds using both datasets (training and testing).

investigation, predicting the scour length (Ls), and scour depth (ds) was done using SVM and GP-based models, which are developed at the junction region of the diversion channel. The performances of the SVM and GP-based best models are recorded and highlighted in Tables 3 and 5 for Ls and ds, respectively, using both training and testing datasets. Agreement plots are plotted in Figures 10 and 11 for a fair comparison among the best models of SVM and GP for Ls prediction and ds during the testing stages, correspondingly. For Ls prediction, Figure 10 and Table 3 confirm that the GP_NPoly models are outperforming SVM-based models. While, for ds prediction, Table 5 and Figure 11 confirm that SVM_Poly is outperforming GP-based models. As presented in Table 7, single-factor ANOVA outcomes display that the *F*-values were fewer than *F*-critical and *P*-values were more than 0.05 suggesting that the difference in predictive values using numerous models and actual values is insignificant. Taylor diagrams are plotted in Figures 12 and 13 for the comparison among the best models

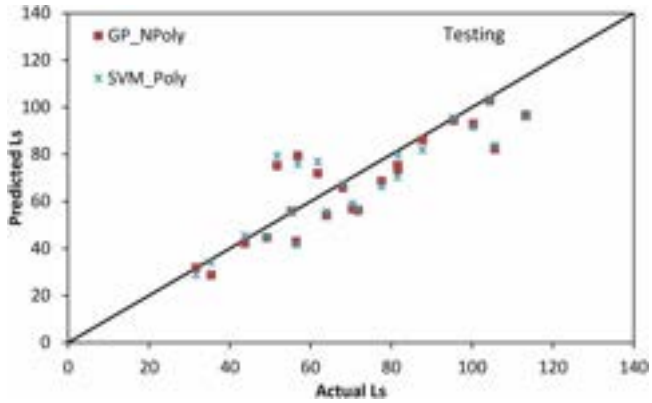

Figure 10 | Agreement plot of outperforming models for Ls prediction using the testing stage.

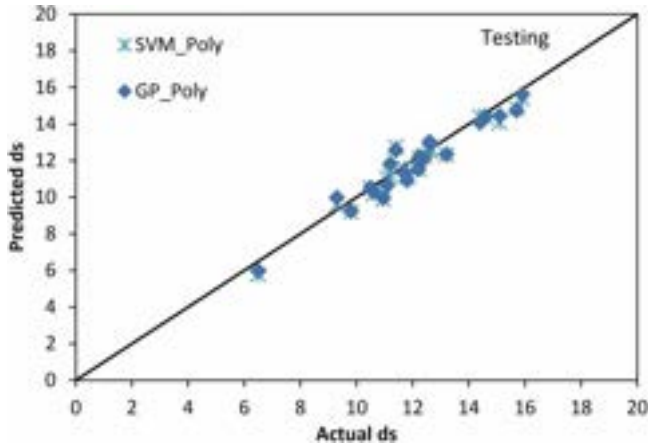

Figure 11 | Agreement plot of outperforming models for ds prediction using the testing stage.

Table 7 | Results of single-factor ANOVA for best-performing models for the prediction of Ls and ds

No.	Source of variation	*F*	*P*-value	*F* crit	Variation among groups
	Ls				
1	Between actual value and SVM_Poly	0.244356	0.623653	4.072654	Insignificant
2	Between actual and GP_NPoly	0.329399	0.569074	4.072654	Insignificant
	ds				
3	Between actual and SVM_Poly	0.210644	0.64863	4.072654	Insignificant
4	Between actual and GP_Poly	0.120739	0.72997	4.072654	Insignificant

for Ls prediction and ds. These figures confirm that GP_NPoly is outperforming other models for Ls prediction and SVM_Poly is outperforming other models for ds prediction.

3.6. Sensitivity investigation

To find the influence of each parameter, which is used for the estimation of the target, sensitivity investigations were performed. Several factors that affect the Ls and ds were included, namely, friction angle (φ), slope angle (β), and stability numbers (m). Best-performing models were employed for this investigation. Performance of the GP_NPoly model with different input combinations was compared performed as presented in Table 8, which suggests that the Sin θ had a significant

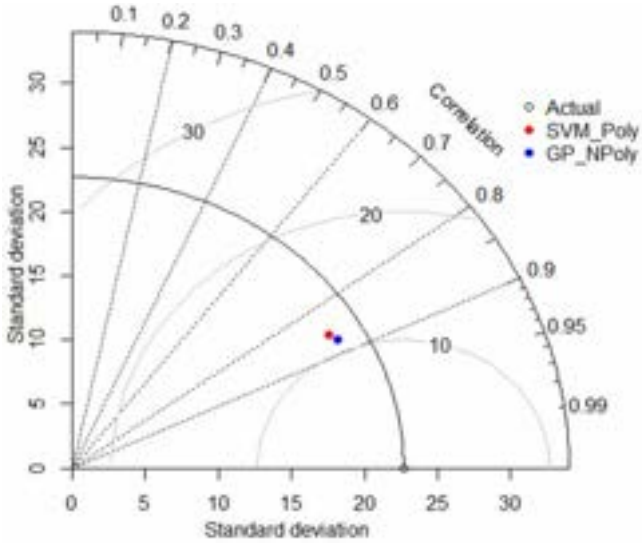

Figure 12 | Taylor plot of outperforming models for Ls prediction using the testing stage.

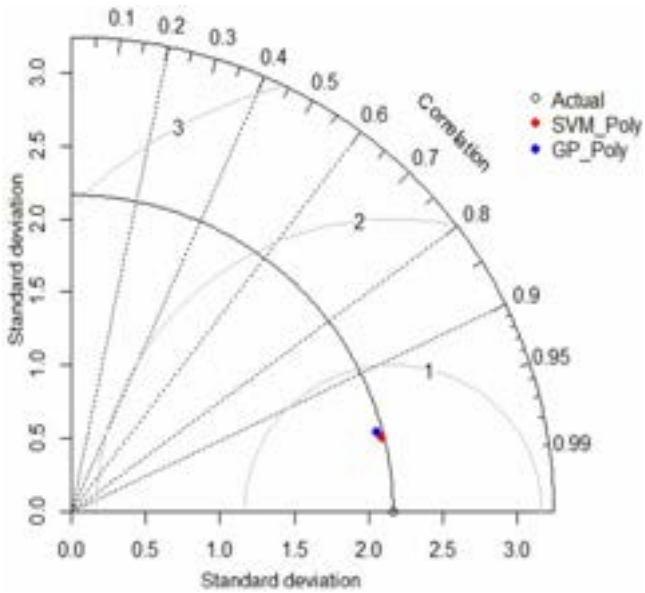

Figure 13 | Taylor plot of outperforming models for ds prediction using the testing stage.

impact on Ls prediction. Table 9 compares the performance of the SVM_Poly model with different input combinations. From Table 9, Sin θ had a significant impact on ds prediction. Overall, Sin θ has a major influence in predicting Ls and ds using this dataset.

4. CONCLUSIONS

The performance of two soft computing techniques (SVM) and (GPR) in predicting scour length and scour depth due to diversion flow was evaluated in this study. Fifteen geometries of the diversion channel represented by five angles of the diversion channel between 30° and 90° and three Br between about 30 and 50% were considered in modeling the diversion flow. In addition, different hydraulic conditions for each model were considered. The investigation used polynomial, normalized polynomial, radial basis, and the Pearson VII kernel function for both SVM and GPR computing techniques. Using different

Table 8 | Sensitivity investigation results for Ls prediction using the GP_NPoly model

Input combination								Output	GP_NPoly model		
Qu	Bb	Vc	Br (%)	Qr	yu	Vu	Sin θ	Ls	CC	RMSE	MAE
■	■	■	■	■	■	■	■	■	0.8744	11.6923	9.0376
□	■	■	■	■	■	■	■	■	0.8777	11.5681	9.0042
■	□	■	■	■	■	■	■	■	0.8746	11.7129	9.0321
■	■	□	■	■	■	■	■	■	0.8722	11.7765	9.1356
■	■	■	□	■	■	■	■	■	0.8746	11.7129	9.0321
■	■	■	■	□	■	■	■	■	0.8645	11.9382	8.9895
■	■	■	■	■	□	■	■	■	0.8760	11.6852	9.0929
■	■	■	■	■	■	□	■	■	0.8560	12.4059	9.3776
■	■	■	■	■	■	■	□	■	0.8349	12.9688	10.3248

Table 9 | Sensitivity investigation results for ds prediction using the SVM_Poly model

Input combination								Output	SVM_Poly model		
Qu	Bb	Vc	Br (%)	Qr	yu	Vu	Sin θ	ds	CC	RMSE	MAE
■	■	■	■	■	■	■	■	■	0.9710	0.6018	0.4530
□	■	■	■	■	■	■	■	■	0.9644	0.6326	0.4639
■	□	■	■	■	■	■	■	■	0.9725	0.5951	0.4591
■	■	□	■	■	■	■	■	■	0.9723	0.5910	0.4617
■	■	■	□	■	■	■	■	■	0.9725	0.5943	0.4579
■	■	■	■	□	■	■	■	■	0.9749	0.5499	0.4332
■	■	■	■	■	□	■	■	■	0.9711	0.6003	0.4541
■	■	■	■	■	■	□	■	■	0.9741	0.5952	0.4839
■	■	■	■	■	■	■	□	■	0.8387	1.2438	0.9644

model performance assessing parameters (CC, MAE, RMSE, NS, and SI) to evaluate the performance of different kernel functions of SVM and GPR computing techniques, the GP_NPoly model was recorded outperforming other models in prediction of Ls and the SVM_Poly model was recorded outperforming the other models in prediction of ds. Sensitivity analysis was undertaken for the input parameters to evaluate the importance of each one for the estimation of the scour length and depth. It suggested that the diversion angle of the diversion channel (θ) has a significant impact on Ls and ds prediction using this dataset. For future work, it is worth conducting further investigation and performing soft computing techniques to predict diversion water and sediment amount.

ACKNOWLEDGEMENTS

Universiti Putra Malaysia funded the experimental tests of this study through its Putra grant (GP-IPS/2015/9453100). The authors extend their sincere gratitude to the University of Mosul.

DATA AVAILABILITY STATEMENT

Data cannot be made publicly available; readers should contact the corresponding author for details.

CONFLICT OF INTEREST

The authors declare there is no conflict.

REFERENCES

Abdalhafedh, A. Y. & Alomari, N. K. 2021 The effect of entrance edges shape of the diversion channel on the dividing streamlines behavior at the junction region. *Al-Rafidain Engineering Journal* **26** (2), 218–226.

Aggarwal, P., Aggarwal, Y., Siddique, R., Gupta, S. & Garg, H. 2013 Fuzzy logic modeling of compressive strength of high-strength concrete (HSC) with supplementary cementitious material. *Journal of Sustainable Cement-Based Materials* **2** (2), 128–143. https://doi.org/10.1080/21650373.2013.801800.

Alomari, N. K., Yusuf, B., Mohammad, T. A. & Ghazali, A. H. 2018 Experimental investigation of scour at a channel junctions of different diversion angles and bed width ratios. *CATENA* **166**, 10–20. https://doi.org/10.1016/j.catena.2018.03.013.

Alomari, N. K., Yusuf, B., Mohammad, T. A. & Ghazali, A. H. 2020 Influence of diversion angle on water and sediment flow into diversion channel. *International Journal of Sediment Research* **35** (6), 600–608. https://doi.org/10.1016/j.ijsrc.2020.06.006.

Amini, S. A., Mohammad, T. A., Aziz, A. A., Ghazali, A. H. & Huat, B. B. K. 2011 A local scour prediction method for pile caps in complex piers. *Proceedings of the Institution of Civil Engineers – Water Management* **164** (2), 73–80.

Amini, A., Melville, B. W., Ali, T. M. & Ghazali, A. H. 2012 Clear-water local scour around pile groups in shallow-water flow. *Journal of Hydraulic Engineering* **138** (2), 177–185. http://dx.doi.org/10.1061/(ASCE)HY.1943-7900.0000488.

Barkdoll, B. D., Ettema, R. & Odgaard, A. J. 1999 Sediment control at lateral diversions: limits and enhancements to vane use. *Journal of Hydraulic Engineering* **125** (8), 862–870. https://doi.org/10.1061/(ASCE)0733-9429(1999)125:8(862).

Cortes, C. & Vapnik, V. 1995 Support-vector networks. *Machine Learning* **20** (3), 273–297.

Dehghani, A. A., Ghodsian, M., Suzuki, K. & Alaghmand, S. 2009 Local Scour Around Lateral Intakes in 180 Degree Curved Channel. In: *Advances in Water Resources and Hydraulic Engineering: Proceedings of 16th IAHR-APD Congress and 3rd Symposium of IAHR-ISHS* (C. Zhang & H. Tang, eds). Springer Berlin Heidelberg, pp. 821–825. https://doi.org/10.1007/978-3-540-89465-0_144.

Dibs, H., Al-Janabi, A. & Gomes, C. 2018 Easy to use remote sensing and GIS analysis for landslide risk assessment. *Journal of University of Babylon for Engineering Sciences* **26** (1), 42–54. Available from: https://www.iasj.net/iasj?func=article&aId=136821.

Duan, J. G., He, L., Fu, X. & Wang, Q. 2009 Mean flow and turbulence around experimental spur dike. *Advances in Water Resources* **32** (12), 1717–1725. https://doi.org/10.1016/j.advwatres.2009.09.004.

Duch, W. 2007 What is computational intelligence and where is it going? In: *Challenges for Computational Intelligence* (W. Duch & J. Mandziuk, eds). Springer, Berlin, Heidelberg, pp. 1–13.

Ehteram, M., Ferdowsi, A., Faramarzpour, M., Al-Janabi, A. M. S., Al-Ansari, N., Bokde, N. D. & Yaseen, Z. M. 2021 Hybridization of artificial intelligence models with nature inspired optimization algorithms for lake water level prediction and uncertainty analysis. *Alexandria Engineering Journal* **60** (2), 2193–2208. https://doi.org/10.1016/j.aej.2020.12.034.

Euler, T. & Herget, J. 2012 Controls on local scour and deposition induced by obstacles in fluvial environments. *CATENA* **91**, 35–46. http://dx.doi.org/10.1016/j.catena.2010.11.002.

Herrero, A., Bateman, A. & Medina, V. 2015 Water flow and sediment transport in a 90° channel diversion: an experimental study. *Journal of Hydraulic Research* **53** (2), 253–263. http://dx.doi.org/10.1080/00221686.2014.989457.

Hoffmans, G. J. C. M. & Pilarczyk, K. W. 1995 Local scour downstream of hydraulic structures. *Journal of Hydraulic Engineering* **121** (4), 326–340. http://dx.doi.org/10.1061/(ASCE)0733-9429(1995)121:4(326.

Hsu, C.-C., Tang, C.-J., Lee, W.-J. & Shieh, M.-Y. 2002 Subcritical 90° equal-width open-channel dividing flow. *Journal of Hydraulic Engineering* **128** (7), 716–720. https://doi.org/10.1061/(ASCE)0733-9429(2002)128:7(716).

Kerssens, P. J. & van Urk, A. 1986 Experimental studies on sedimentation due to water withdrawal. *Journal of Hydraulic Engineering* **112** (7), 641–656. https://doi.org/10.1061/(ASCE)0733-9429(1986)112:7(641).

Keshavarzi, A. & Habibi, L. 2005 Optimizing water intake angle by flow separation analysis. *Irrigation and Drainage* **54** (5), 543–552. https://doi.org/10.1002/ird.207.

Khwairakpam, P. & Mazumdar, A. 2009 Local scour around hydraulic structures. *International Journal of Recent Trends in Engineering* **1** (6), 59.

Kleinhans, M. G., Ferguson, R. I., Lane, S. N. & Hardy, R. J. 2013 Splitting rivers at their seams: bifurcations and avulsion. *Earth Surface Processes and Landforms* **38** (1), 47–61. https://doi.org/10.1002/esp.3268.

Kuss, M. 2006 *Gaussian Process Models for Robust Regression, Classification, and Reinforcement Learning*. PhD Thesis. Technische Universität Darmstadt Darmstadt, Germany.

Liu, P., Choo, K.-K. R., Wang, L. & Huang, F. 2017 SVM or deep learning? A comparative study on remote sensing image classification. *Soft Computing* **21** (23), 7053–7065. https://doi.org/10.1007/s00500-016-2247-2.

Mehdipour, V., Stevenson, D. S., Memarianfard, M. & Sihag, P. 2018 Comparing different methods for statistical modeling of particulate matter in Tehran, Iran. *Air Quality, Atmosphere & Health* **11** (10), 1155–1165. https://doi.org/10.1007/s11869-018-0615-z.

Michell, F., Ettema, R. & Muste, M. 2006 Case study: sediment control at water intake for large thermal-power station on a small river. *Journal of Hydraulic Engineering* **132** (5), 440–449. https://doi.org/10.1061/(ASCE)0733-9429(2006)132:5(440).

Mignot, E., Zeng, C., Dominguez, G., Li, C.-W., Rivière, N. & Bazin, P.-H. 2013 Impact of topographic obstacles on the discharge distribution in open-channel bifurcations. *Journal of Hydrology* **494**, 10–19. http://dx.doi.org/10.1016/j.jhydrol.2013.04.023.

Mignot, E., Doppler, D., Riviere, N., Vinkovic, I., Gence, J.-N. & Simoens, S. 2014 Analysis of flow separation using a local frame axis: application to the open-channel bifurcation. *Journal of Hydraulic Engineering* **140** (3), 280–290. http://dx.doi.org/10.1061/(ASCE)HY.1943-7900.0000828.

Momplot, A., Lipeme Kouyi, G., Mignot, E., Rivière, N. & Bertrand-Krajewski, J.-L. 2017 Typology of the flow structures in dividing open channel flows. *Journal of Hydraulic Research* **55** (1), 63–71. http://dx.doi.org/10.1080/00221686.2016.1212409.

Moradi, F., Bonakdari, H., Kisi, O., Ebtehaj, I., Shiri, J. & Gharabaghi, B. 2019 Abutment scour depth modeling using neuro-fuzzy-embedded techniques. *Marine Georesources & Geotechnology* **37** (2), 190–200. https://doi.org/10.1080/1064119X.2017.1420113.

Nakato, T. 1984 *Model Investigation of Intake-Shoaling and Pump-Vibration Problems: Iowa Generation Council Bluffs Unit 3 Circulating-Water Intake*. Report No. 283 Iowa Institute of Hydraulic Research, University of Iowa, Iowa.

Nakato, T. & Ogden, F. L. 1998 Sediment control at water intakes along sand-bed rivers. *Journal of Hydraulic Engineering* **124** (6), 589–596. https://doi.org/10.1061/(ASCE)0733-9429(1998)124:6(589).

Nakato, T., Kennedy, J. F. & Bauerly, D. 1990 Pump-station intake-shoaling control with submerged vanes. *Journal of Hydraulic Engineering* **116** (1), 119–128. https://doi.org/10.1061/(ASCE)0733-9429(1990)116:1(119).

Neal, R. M. 2000 Markov chain sampling methods for Dirichlet process mixture models. *Journal of Computational and Graphical Statistics* **9** (2), 249–265.

Pagliara, S., Kurdistani, S. M., Palermo, M. & Simoni, D. 2016 Scour due to rock sills in straight and curved horizontal channels. *Journal of Hydro-Environment Research* **10**, 12–20. http://dx.doi.org/10.1016/j.jher.2015.07.002.

Ramamurthy, A. S. & Satish, M. G. 1988 Division of flow in short open channel branches. *Journal of Hydraulic Engineering* **114** (4), 428–438. https://doi.org/10.1061/(ASCE)0733-9429(1988)114:4(428).

Ramamurthy, A. S., Minh Tran, D. & Carballada, L. B. 1990 Dividing flow in open channels. *Journal of Hydraulic Engineering* **116** (3), 449–455. https://doi.org/10.1061/(ASCE)0733-9429(1990)116:3(449).

Redolfi, M., Zolezzi, G. & Tubino, M. 2016 Free instability of channel bifurcations and morphodynamic influence. *Journal of Fluid Mechanics* **799**, 476–504. https://doi.org/10.1017/jfm.2016.389.

Seyedian, S. M., Bajestan, M. S. & Farasati, M. 2014 Effect of bank slope on the flow patterns in river intakes. *Journal of Hydrodynamics* **26** (3), 482–492. http://dx.doi.org/10.1016/S1001-6058(14)60055-X.

Sihag, P., Singh, B., Gautam, S. & Debnath, S. 2018 Evaluation of the impact of fly ash on infiltration characteristics using different soft computing techniques. *Applied Water Science* **8** (6), 187. https://doi.org/10.1007/s13201-018-0835-2.

Sihag, P., Singh, V. P., Angelaki, A., Kumar, V., Sepahvand, A. & Golia, E. 2019 Modelling of infiltration using artificial intelligence techniques in semi-arid Iran. *Hydrological Sciences Journal* **64** (13), 1647–1658. https://doi.org/10.1080/02626667.2019.1659965.

Sihag, P., Al-Janabi, A. M. S., Alomari, N. K., Ghani, A. A. & Nain, S. S. 2021 Evaluation of tree regression analysis for estimation of river basin discharge. *Modeling Earth Systems and Environment* **7** (4), 2531–2543. https://doi.org/10.1007/s40808-020-01045-9.

Smola, A. J. 1996 *Regression Estimation with Support Vector Learning Machines*. Master's Thesis, Technische Universität München, Germany.

Solaimani, N., Amini, A., Banejad, H. & Taherei Ghazvinei, P. 2017 The effect of pile spacing and arrangement on bed formation and scour hole dimensions in pile groups. *International Journal of River Basin Management* **15** (2), 219–225. https://doi.org/10.1080/15715124.2016.1274321.

Taylor, K. E. 2001 Summarizing multiple aspects of model performance in a single diagram. *Journal of Geophysical Research: Atmospheres* **106** (D7), 7183–7192.

Taylor, C. & Meldrum, D. 1994 Freeway traffic data prediction via artificial neural networks for use in a fuzzy logic ramp metering algorithm. In: *Proceedings of the Intelligent Vehicles '94 Symposium* IEEE (Anon, ed.). Piscataway, NJ, USA, pp. 308–313.

Williams, C. K. & Rasmussen, C. E. 2006 *Gaussian Processes for Machine Learning*. MIT press Cambridge, MA.

Xu, M., Chen, L., Wu, Q. & Li, D. 2016 Morph- and hydro-dynamic effects toward flood conveyance and navigation of diversion channel. *International Journal of Sediment Research* **31** (3), 264–270. http://dx.doi.org/10.1016/j.ijsrc.2015.09.001.

Yaseen, Z. M., Sihag, P., Yusuf, B. & Al-Janabi, A. M. S. 2021 Modelling infiltration rates in permeable stormwater channels using soft computing techniques. *Irrigation and Drainage* **70** (1), 117–130. https://doi.org/10.1002/ird.2530.

Yetilmezsoy, K., Sihag, P., Kıyan, E. & Doran, B. 2021 A benchmark comparison and optimization of Gaussian process regression, support vector machines, and M5P tree model in approximation of the lateral confinement coefficient for CFRP-wrapped rectangular/square RC columns. *Engineering Structures* **246**, 113106. https://doi.org/10.1016/j.engstruct.2021.113106.

First received 6 October 2022; accepted in revised form 25 December 2022. Available online 4 February 2023